



University for the Common Good

Retinal pigment epithelium cholesterol efflux mediated by the 18kDa translocator protein, TSPO, a potential target for treating age-related macular degeneration

Biswas, Lincoln; Zhou, Xinzhi; Dhillon, Baljean ; Graham, Annette; Shu, Xinhua

Published in:

Human Molecular Genetics

DOI:

[10.1093/hmg/ddx319](https://doi.org/10.1093/hmg/ddx319)

Publication date:

2017

Document Version

Peer reviewed version

[Link to publication in ResearchOnline](#)

Citation for published version (Harvard):

Biswas, L, Zhou, X, Dhillon, B, Graham, A & Shu, X 2017, 'Retinal pigment epithelium cholesterol efflux mediated by the 18kDa translocator protein, TSPO, a potential target for treating age-related macular degeneration', *Human Molecular Genetics*, vol. 26, no. 22, pp. 4327–4339. <https://doi.org/10.1093/hmg/ddx319>

General rights

Copyright and moral rights for the publications made accessible in the public portal are retained by the authors and/or other copyright owners and it is a condition of accessing publications that users recognise and abide by the legal requirements associated with these rights.

Take down policy

If you believe that this document breaches copyright please view our takedown policy at <https://edshare.gcu.ac.uk/id/eprint/5179> for details of how to contact us.

1 **Retinal pigment epithelium cholesterol efflux mediated by the 18kDa translocator protein,**
2 **TSPO, a potential target for treating age-related macular degeneration**

3 Lincoln Biswas¹, Xinzhi Zhou¹, Baljean Dhillon², Annette Graham¹, Xinhua Shu^{1*}

4 1. Department of Life Sciences, Glasgow Caledonian University, Cowcaddens Road, Glasgow G4
5 0BA

6 2. Centre for Clinical Brain Sciences, University of Edinburgh, Edinburgh EH16 4SB

7

8 * To whom correspondence should be addressed at: Department of Life Sciences, Glasgow
9 Caledonian University, Glasgow G4 0BA. Tel: +44 1413318763; Fax: +44 141 3313208; Email:

10 Xinhua.Shu@gcu.ac.uk

11

12

13

14

15

16

17

18

19

20

21

22

23

24

25

26

27

28

29 **Abstract**

30 Cholesterol accumulation beneath the retinal pigment epithelium (RPE) cells is supposed to contribute
31 the pathogenesis of age-related macular degeneration (AMD). Cholesterol efflux genes (*APOE* and
32 *ABCA1*) were identified as risk factors for AMD, although how cholesterol efflux influences
33 accumulation of this lipid in sub-RPE deposits remains elusive. The 18kDa translocator protein,
34 TSPO, is a cholesterol-binding protein implicated in mitochondrial cholesterol transport. Here, we
35 investigate the function of TSPO in cholesterol efflux from the RPE cells. We demonstrate in RPE
36 cells that TSPO specific ligands promote cholesterol efflux to acceptor (apo)lipoprotein and human
37 serum, while loss of TSPO resulted in impaired cholesterol efflux. *TSPO*^{-/-} RPE cells also had
38 significantly increased production of reactive oxygen species (ROS) and upregulated expression of
39 proinflammatory cytokines (IL-1 β and TNF α). Cholesterol (oxidized LDL) uptake and accumulation
40 were markedly increased in *TSPO*^{-/-} RPE cells. Finally, in aged RPE cells, TSPO expression was
41 reduced and cholesterol efflux impaired. These findings provide a new pharmacological concept to
42 treat early AMD patients by stimulating cellular cholesterol removal with TSPO specific ligands or by
43 overexpression of TSPO in RPE cells.

44 **Keywords** TSPO, cholesterol efflux, retinal pigment epithelium cell (RPE), age-related macular
45 degeneration

46

47

48

49

50

51

52

53

54

55

56

57 **Introduction**

58 Age-related macular degeneration (AMD) is the commonest cause of registered blindness in the
59 developed world (1). An important clinical feature of AMD is the accumulation of both focal
60 (Drusen) and diffuse extracellular (basal) deposits in the macula, between the retinal pigment
61 epithelium (RPE) and the adjacent Bruch's membrane. One current hypothesis is that these deposits
62 lead to dysfunction and later death of RPE and associated loss of photoreceptors (2). Ageing is
63 associated with progressive accumulation of lipids within Bruch's membrane (3). Lipid deposition
64 causes hydraulic conductivity and macromolecular permeability in Bruch's membrane, which is
65 thought to impair retinal metabolism. Histopathological analyses of AMD patients' eyes have
66 demonstrated the presence of apolipoproteins, cholesterol and cholesteryl ester deposits underneath
67 the RPE, implicating abnormal cholesterol transport in the progression of this disease (4). Genome
68 wide association studies have also implicated that hepatic lipase C (*LIPC*) and cholesteryl ester
69 transfer protein (*CETP*), key genes involved in the metabolism of triglycerides and high-density
70 lipoproteins (HDL), in the pathogenesis of AMD (5,6).

71 Excess cholesterol is removed from peripheral cells by the reverse cholesterol transport (RCT)
72 pathway, by which HDL return excess cellular cholesterol to the liver for either storage as cholesteryl
73 ester droplets or for excretion in bile. Cholesterol efflux is the first step in RCT mediated by the
74 removal of cholesterol by acceptors, such as (apo)lipoproteins. Cholesterol efflux is mediated by
75 ATP-binding cassette (ABC) transporters, such as ABCA1, ABCG1 and ABCG4 (7). Our previous
76 work in human macrophages has established that increased mitochondrial cholesterol trafficking, via
77 the 18kDa translocator protein (TSPO), can enhance expression of key genes encoding proteins
78 involved in the cholesterol efflux pathway, and facilitate removal of cholesterol by apolipoprotein
79 acceptors (8). Transfer of cholesterol to mitochondrial sterol 27-hydroxylase (*CYP27A1*) increases
80 generation of oxysterol ligands for Liver X receptors, which induce the expression of ABCA1,
81 ABCG1/4 and ApoE.

82 Mitochondrial cholesterol trafficking is thought to involve a complex of proteins including TSPO,
83 steroidogenic acute regulatory protein (StAR), the voltage dependent anion channel (VDAC) and
84 possibly the adenine nucleotide channel (ANC), together with putative regulatory proteins (9). The

85 TSPO protein, previously called the peripheral-type benzodiazepine receptor, is an 18kDa
86 transmembrane protein localized in the outer mitochondrial membrane of different tissues. TSPO is
87 thought to mediate a number of functions, including cholesterol transport, steroidogenesis,
88 neuroinflammation, prevention of apoptosis, and stress adaptation (9). Global or conditional *Tspo*
89 knockout (KO) mouse models have been reported; the KO mice exhibited divergent phenotypes
90 (embryonic lethal, defect in steroidogenesis, or no effect on steroidogenesis) possibly due to genetic
91 background differences between strains of those KO mice (10-12).

92 The RCT process may be important in the pathogenesis of AMD because of its involvement in
93 lipid and cholesterol transport from RPE (13). The RPE cells are involved in phagocytosis and
94 degradation of photoreceptor outer segments (POS), which are thought to be the major source of
95 excess RPE lipids. Incompletely digested POS lipids accumulate as autofluorescent lipid-protein
96 aggregates called lipofuscin in RPE. Retinoid metabolites, such as bis-retinoids, also contribute to the
97 formation of lipofuscin (14). About 20% of RPE cell volume is occupied by lipofuscin by the age of
98 80 years (15). Notably, the lipofuscin fluorophore A2E blocks cholesterol efflux, resulting in the
99 accumulation of both free cholesterol and cholesteryl esters in RPE cells (14). Further, RPE cells have
100 been shown to express ABCA1, scavenger receptor BI (SR-BI), apolipoprotein A-I (ApoA-I), and
101 apolipoprotein E (ApoE), which participate in the RCT process (16); ABCA1 and ApoE are also
102 associated with susceptibility to AMD (6, 17). ApoE is synthesized and secreted by RPE cells in
103 considerable amounts comparable to those in the liver and brain, the two most abundant biological
104 synthetic sources of ApoE (18). ApoE and ApoA-I proteins were detected in drusen and have been
105 implicated in apolipoprotein-mediated RCT in lipid trafficking and in facilitating the efflux of lipids
106 from the RPE, and their transit across Bruch's membrane to the choroidal vasculature (19).

107 There have been no previous studies investigating the function of the mitochondrial cholesterol
108 trafficking protein, TSPO, in RPE cells. In this study, we found TSPO to be highly expressed in
109 human RPE (ARPE-19 cell line) and mouse RPE cells. We also found TSPO ligands significantly
110 increased cholesterol efflux to ApoE, ApoA-I and HDL from RPE cells. When TSPO was deleted in
111 RPE cells, TSPO-specific ligand treatment could not increase cholesterol efflux. Aged mouse RPE
112 cells had significantly decreased *Tspo* expression and impaired cholesterol efflux. Our observations

113 demonstrated that TSPO is involved in regulating cholesterol efflux from RPE cells, suggesting TSPO
114 as a potential therapeutic target for AMD.

115

116 **Results**

117 **TSPO ligands increased cholesterol efflux from RPE cells**

118 Previously reports showed that TSPO, a mitochondrial outer membrane protein, is expressed in
119 fibroblasts, macrophages, microglia and astrocytes (8, 20-25). We examined TSPO expression in
120 ARPE-19 cells using a rabbit monoclonal antibody and found TSPO to be present and localized to
121 mitochondria (Fig. 1). Initially, human ARPE-19 cells were treated with a range of TSPO ligands at
122 different concentrations (2.5 to 30 μ M), compared with the vehicle control, to determine the highest
123 concentration that does not significantly affect the viability of ARPE-19 cells over 24 hours treatment.
124 The suitable concentration of each ligand was identified as FGIN-1-27 (10 μ M), XBD173 (25 μ M)
125 and Etifoxine (20 μ M) respectively (Supplementary Material, Fig. S1).

126 Previous reports demonstrated that TSPO regulated cholesterol efflux in fibroblast and
127 macrophage cells (8, 21). We treated ARPE-19 cells with TSPO specific ligands for 24 hours and
128 found that FGIN-1-27 and XBD173 significantly increased cholesterol efflux to apoE, apoA-I, HDL,
129 and human serum (HS), and Etifoxine significantly increased cholesterol efflux to HDL and HS (Fig.
130 2).

131

132 **Ligands of TSPO decreased lipogenesis in RPE cells**

133 We investigated whether treatment of TSPO ligand affected lipogenesis in ARPE-19 cells by
134 measuring the syntheses of phospholipid, triacylglycerol, cholesteryl and fatty acid. We found
135 significantly reduced incorporation of [14 C]acetate into phospholipid by 30% in FGIN-1-27 treated
136 cells and by 36% in XBD173 treated cells. Incorporation of [14 C]acetate into free cholesterol pools
137 was also significantly decreased by 35% in FGIN-1-27 treated cells and by 31.52% in XBD173
138 treated cells, compared with the vehicle control (Fig. 3A, B). By contrast, there was no significant
139 difference when incorporation of [14 C]acetate into triglycerides, fatty acid and cholesterol ester pools
140 between ligand-treated and control cells were compared (Fig. 3A and B). Etifoxine-treated ARPE-19

141 cells exhibited significant reduction by 57.42% in incorporation of [¹⁴C]acetate into the free
142 cholesterol pool compared with the vehicle control; the other examined lipid pools showed no
143 significant changes for the same comparison (Fig. 3C). We also measured total cholesterol mass and
144 phospholipids in control and ligand treated ARPE-19 cells and found significant reduction in total
145 cholesterol by 35.49%, 32.51% and 23.61% in FGIN-1-27, XBD173 and Etifoxine treated cells,
146 respectively (Fig. 3D) and in phospholipid contents by 29.18% and 9.93% in FGN1-27 and XBD173
147 treated cells respectively (Fig. 3E).

148

149 **Ligands of TSPO increased gene expression of proteins involved in cholesterol transport and** 150 **metabolism in RPE cells**

151 Since treatment with TSPO ligands influenced cholesterol efflux (Fig. 2), we examined expression of
152 genes involved in cholesterol homeostasis in ARPE-19 cells that were treated with FGIN-1-27
153 (10µM), XBD173 (25 µM) or Etifoxine (20 µM) for 24 hours. The mRNA expression levels of these
154 genes relative to housing keeping gene *GAPDH* were shown in Supplementary Material, Fig. S2A.
155 FGIN-1-27 significantly upregulated the expression of *NR1H3* (encoding to liver X receptor alpha
156 protein, *LXRα*), *ABCA1*, *ABCG1* and *CYP27A1* but not *CYP46A1* (Supplementary Material, Fig.
157 S2A), while Etifoxine notably enhanced the expression of *LXRα*, *ABCA1*, *ABCG1* and *CYP46A1*
158 except *CYP27A1* (Supplementary Material, Fig. S2A). XBD173 significantly increased expression of
159 all examined genes when compared to the vehicle controls (Supplementary Material, Fig. S2A). We
160 also assessed protein levels of *LXRα*, *ABCG1*, *ABCA1*, *CYP27A1* and *CYP46A1* in ARPE-
161 19 treated with TSPO ligands, by Western blotting (Supplementary Material, Fig. S2B). FGIN-
162 1-27 treatment resulted in significant increases of *LXRα*, *ABCG1* and *ABCA1* proteins,
163 compared with the vehicle controls, but the trend towards increased expression of *CYP27A1*
164 and *CYP46A1* proved non-significant (Supplementary Material, Fig. S2C). Etifoxine treatment
165 caused notable increases in expression of *ABCG1* and *CYP46A1* protein, but no significant
166 increases in *LXRα*, *ABCA1* and *CYP27A1* proteins were observed, compared with the
167 vehicle controls (Supplementary Material, Fig. S2C). Incubation with XBD173 significantly

168 increased the levels of LXR α , ABCG1, CYP27A1 and CYP46A1 proteins, but did not
169 significantly alter the levels of ABCA1 protein (Supplementary Material, Fig. S2C).

170

171 **Knockout of *TSPO* in RPE cells using the CRISPER/Cas9 engineering system**

172 Human *TSPO* gene contains four exons with exon 1 untranslated (Fig. 4A). To delete *TSPO*, we
173 followed the protocol of the CRISPR/Cas9 system and designed a guide RNA (gRNA) having
174 sequence complementary to 18 nucleotides (c.87_104) of *TSPO* exon 2 (Fig. 4A). ARPE-19 cells
175 were transfected with the gRNA construct and the Cas9 expression plasmid. Nine colonies were
176 derived from G418 transient selection. Two colonies, named KO1 and KO2, with loss of *TSPO* were
177 confirmed by Western blotting using a *TSPO*-specific antibody (Fig. 4B). Immunocytochemistry
178 further confirmed *TSPO* was absent from KO1 and KO2 cells (Fig. 4C). We used Sanger Sequencing
179 to find that KO1 had an insertion of 82 bp (cc.101_102ins82.) and KO2 contained a deletion of 8 bp
180 (c.96_103del8) in the target region of exon 2 (Fig. 4A). The deletion/insertion mutations resulted in
181 frame-shift reading with truncated peptides (Supplementary Material, Fig. S3).

182

183 **Increased lipid accumulation in *TSPO* knockout RPE cells**

184 Treatment with *TSPO* specific ligands enhanced cholesterol efflux in ARPE-19 cells (Fig. 2).
185 However, when *TSPO* was deleted, the knockout cells had no significant change in [³H]cholesterol
186 efflux to apoE, apoA-I, HDL, or human serum after treatment with FGIN-1-27, XBD173 or Etifoxine
187 (Supplementary Material, Fig. S4). We therefore investigated whether loss of *TSPO* in APRE-19 cells
188 cause lipid accumulation. When wildtype and *TSPO*^{-/-} cells were incubated with DiI-OxLDL for 24
189 hours we found intracellular OxLDL were significantly increased in *TSPO*^{-/-} cells by 39% (p<0.01)
190 compared to wildtype cells (Fig. 5A, B). We also confirmed significant increase of OxLDL
191 accumulation in *TSPO* deleted RPE cells using fluorescence-activated cell sorting assay (Fig. 5C) .We
192 determined whether the increase of OxLDL accumulation was also related oxLDL uptake in *TSPO*^{-/-}
193 cells, we fed both wildtype and *TSPO*^{-/-} cells with DiI-OxLDL for 4 hours and assessed intracellular

194 oxLDL by confocal imaging and FACS assay. We found that uptake of OxLDL was significantly
195 increased by 34% in TSPO deleted cells (Fig. 5D, E, F).

196 Previous data showed uptake of LDL and OxLDL by rodent RPE cells occurs primarily via LDL
197 receptor (LDLR) (26), which is expressed in both rodent and human RPE cells (26, 27). We used
198 qRT-PCR and Western blotting to assess the level of LDLR in wildtype and TSPO deleted cells
199 loaded with OxLDL. The *LDLR* mRNA level in *TSPO*^{-/-} cells incubated with oxLDL for 4 h and 24 h
200 was significantly increased by 2341 fold and 1501 fold, respectively, when compared to that of
201 wildtype cells (Fig. 6A, C). Expression of LDLR protein also increased significantly in *TSPO*^{-/-} cells
202 when compared to wildtype cells (Fig. 6B, D). Intracellular OxLDL cause increased oxidative stress,
203 promoting the production of inflammatory cytokines, IL-1 β and TNF α , that enhance LDLR
204 expression (28-30). We therefore measured reactive oxygen species (ROS) production in both
205 wildtype and *TSPO*^{-/-} RPE cells cultured in serum-free medium or in serum-free medium with
206 OxLDL. When cultured in serum-free medium, *TSPO*^{-/-} cells produced significantly higher level of
207 ROS at 4 and 24 hours by 39% and 52% respectively (Fig. 7A, B), consistent with early report that
208 deletion of TSPO increased ROS production in steroidogenic cells (31). Both wildtype and TSPO-
209 deleted RPE cells incubated with OxLDL had marked increase of ROS production at 4 and 24 h when
210 compared to cells cultured in serum-free medium, indicating oxLDL promoted ROS production. In
211 the presence of OxLDL, *TSPO*^{-/-} cells also had significant increase of ROS production when
212 compared to wildtype RPE cells at 4 and 24 h by 64% and 58% respectively (Fig. 7A, B).

213 We also measured the secretion of IL-1 β and TNF α into the media above wildtype and TSPO-
214 deleted cells by enzyme-linked immunosorbent assay (ELISA). When cultured in serum-free medium,
215 *TSPO*^{-/-} cells exhibited a trend towards increased output of IL-1 β at 4 and 24 hours though there was
216 no significant difference compared to wildtype cells. However, TNF α levels were increased in the
217 media above *TSPO*^{-/-} cells by 37%, with a significant difference noted from the wildtype control at 24
218 hours (Fig. 7C, D). Levels of both IL-1 β and TNF α were markedly higher in *TSPO*^{-/-} cells compared
219 to wildtype cells when incubated with oxLDL at 4 and 24 h (Fig. 7C, D). Further, when wildtype and
220 *TSPO*^{-/-} RPE cells were treated with IL-1 β (10ng/ml) or TNF α (50ng/ml) for 4 hours, the level of
221 LDLR protein was significantly, if modestly, increased in TSPO-deleted cells; when treated for 24

222 hours with these cytokines, LDLR protein levels were significantly increased in both wildtype and
223 *TSPO*^{-/-} cells (Supplementary Materials, Fig. S5).

224

225 **Reduced TSPO expression and impaired cholesterol efflux in aged mouse RPE cells**

226 Wang et al (2015) examined TSPO localization in developmental and young adult mouse retina and
227 showed TSPO was localized in the developing and migratory microglia at P0, P3 and P7, while the
228 localization in microglia disappeared at P14. At P28 (young adult), TSPO signal was detected only in
229 retinal blood vessels and not in any other retinal cells, however TSPO protein was gradually increased
230 during retinal development with significant high level in young adult retina (25). We performed
231 immunostaining to detect TSPO expression in the retinas of adult mice (3 months old) and found a
232 marked strong signal in RPE cell layer, and quite a strong signal presented in the ganglion cell layer
233 (Fig. 8A, B). We also detected TSPO immunopositivity in the choroid, possibly in the choroid
234 vessels. We quantified the expression of *Tspo* mRNA and protein in mouse retina and RPE/choroid:
235 *Tspo* mRNA level in RPE/choroid was 20.7 fold higher than that in the retina, TSPO protein level in
236 RPE/choroid was 16.7 fold higher than that in the retina (Fig. 8C-E).

237 We further investigated TSPO expression in aged mouse RPE and retina: TSPO was significantly
238 decreased by 58.67% at mRNA level and by 24.46% at protein level in 20-month old mouse RPE
239 cells when compared to that of 3-month old RPE cells (Fig. 9A-C). Expression of the cholesterol
240 transporter genes, *Abca1* and particularly *Abcg1*, in aged RPE was also significantly decreased
241 (Supplementary Material, Fig. S6A). In aged mouse retina, we also detected significantly declined
242 expression of *Tspo*, *Abca1* and *Abcg1* (Supplementary Material, Fig. S6B).

243 The total cholesterol mass was measured in 3-month and 20-month old mouse RPE and that the
244 cholesterol mass of 20-month old RPE was significantly higher than that of 3 moth-old RPE/choroid
245 (Fig. 9D). We therefore investigated whether the increase of total cholesterol in aged RPE is partially
246 due to a defect in cholesterol efflux. We observed that the percentage of [³H]cholesterol efflux to
247 apoE, apoA-I, HDL, or human serum was significantly decreased in 20-months old RPE when
248 compared to that of 3-months old RPE (Fig. 9E).

249

250 **Discussion**

251 Extensive clinical studies show abnormal cholesterol accumulation in drusen of AMD patients,
252 implicating dysregulated cholesterol homeostasis (32). Experimental research has demonstrated that
253 impaired cholesterol efflux might contribute to the pathogenesis of AMD (15,33). However the
254 underlying mechanisms are not fully understood. The present study demonstrated that TSPO ligands
255 enhance cholesterol efflux in RPE cells. Deletion of TSPO prevented modulation on cholesterol efflux
256 by TSPO ligands and resulted in markedly increased cholesterol (OxLDL) uptake and accumulation in
257 TSPO^{-/-} RPE cells. Aged mice had significant decrease in retinal and RPE expression of TSPO and
258 defective cholesterol efflux in aged primary RPE cells.

259 TSPO is an outer mitochondrial membrane (OMM) protein with five transmembrane (TM) helices
260 and can bind cholesterol at a high affinity through its C-terminal cholesterol recognition amino acid
261 consensus (CRAC) motif to transport cholesterol to the inner mitochondrial membrane (IMM) (34,
262 35). TSPO can also bind different ligands, which promote cholesterol movement from OMM to
263 IMM, where cholesterol is converted into pregnenolone by CYP11A1 in steroidogenic tissues or into
264 oxysterols (27-hydroxycholesterol and 5-cholestanoic acid) by CYP27A1 in macrophage and other cell
265 types (34). Oxysterols can activate a nuclear transcription factor, liver X receptor (LXR α/β), thereby
266 upregulating the transcription of ABCA1, ABCG1 and ABCG4, which promote cholesterol efflux. In
267 ARPE-19 cells, TSPO specific-ligands enhanced the efflux of cholesterol to ApoA-I, apoE and HDL
268 (Fig. 2) and markedly decreased the total cholesterol level, and the biogenesis of free cholesterol (Fig.
269 3). Equally, TSPO ligand treatment significantly increased expression of ABCA1, ABCG1 and LXR α
270 (Supplementary Material, Fig. S2). CYP27A1 was localised in human RPE (27) and its expression
271 was significantly increased in RPE cells exposed to TSPO specific ligands FGIN-1-27 or XBD173
272 (Supplementary Materials, Fig. 3). Our data suggested TSPO has similar function in cholesterol efflux
273 in RPE cells possibly through oxysterol activated LXR-mediated upregulation of cholesterol
274 transporter genes and down-regulation of cholesterol biosynthesis.

275 Apolipoprotein-containing lipoproteins accumulate and become oxidized in drusen (36).
276 Apolipoprotein B100 (apoB100) is the major apolipoprotein of LDL, and oxidized apoB100 and
277 OxLDL localized in drusen (37). Early data showed OxLDL was internalized by RPE cells, causing a

278 defect in outer segment phagocytosis and induced apoptosis (37-40). Recent data demonstrated
279 OxLDL triggered the alternative complement pathway by decreasing complement regulator CD59 and
280 increasing the formation of membrane attack complexes (MACs) in RPE cells (41,42). Our
281 experiments indicated that deletion of TSPO enhance OxLDL uptake and accumulation in RPE cells
282 (Fig. 5), which may contribute to abnormal outer segment phagocytosis and dysfunction of the
283 alternative complement system. Certainly, loss of TSPO caused increased oxidative stress in RPE
284 cells by producing higher level of ROS (Fig. 7A, B) and secretion of IL-1 β and TNF α levels was
285 markedly increased in OxLDL-treated *TSPO*^{-/-} RPE cells (Fig. 7C, D). When ARPE-19 cells were
286 exposed to IL-1 β or TNF α , the expression of LDLR was significantly upregulated (Supplementary
287 Material, Fig. S5), which promotes OxLDL uptake. ROS also can oxidatively modify macromolecules
288 such as DNA, protein and lipid and lead to dysfunction of RPE cells. Together, these data suggest that
289 loss of TSPO contributes to both dysregulated cholesterol metabolism and inflammation, and may
290 play a central in the pathogenesis of AMD.

291 TSPO is upregulated in activated microglial cells of different neurodegenerative diseases and
292 recognized as a biomarker for early diagnosis and disease progression (43); TSPO expression was
293 significantly increased at mRNA and protein level in retinal microglial cells by LPS-induced
294 inflammation (25, 44). TSPO was also strongly upregulated in retinal microglia in models of retinal
295 injury and degeneration (25, 44). Knockdown of TSPO significantly increased ROS production and
296 TNF α secretion in microglial cells (BV2) in response to LPS challenge; there was no significant
297 increase of ROS production and TNF α expression in knockdown cells without LPS-activation,
298 possibly due to only 30-40% TSPO depletion (44). In this study, TSPO knockout RPE cells had
299 significant increase in the production of ROS and in secretion of IL-1 β and TNF α (Fig. 7C,D). TSPO
300 ligand (PK-11195 and Ro5-4864) treatment significantly decreased ROS production and TNF α
301 secretion in BV2 cells; intravitreal treatment with a TSPO ligand (TTN) inhibited LPS-induced retinal
302 inflammatory reaction by reducing retinal lipid peroxidation and TNF α protein level (25). Treatment
303 with another TSPO ligand, XBD173, reduced expression of pro-inflammatory genes and prevented
304 photoreceptor cell death in light-induced retinal degeneration (45). We also found treatment with

305 TSPO ligands significantly down-regulated expression of pro-inflammatory cytokines in ARPE-19
306 cells (data not shown).

307 Previous reports showed that TSPO was localized to retinal microglia and inner retinal blood
308 vessels (25, 44). We found very strong TSPO signal in three-month old mouse RPE cells, less strong
309 signal in the choroid and some weak signals in the inner and outer plexiform layers (possibly the
310 microglia); we also found quite strong signals in ganglion cells (Fig. 8A, B). Ishikawa et al reported
311 that increased pressure could upregulate TSPO expression in rat ganglion cells; TSPO was
312 undetectable at 10 mmHg and significantly increased in ganglion cells at 35 mmHg and 75 mmHg
313 respectively (46). The difference of immunolocalization of TSPO in retina was possibly due to
314 different approaches for preparing immunostaining samples or immunodetection methods. We used
315 qRT-PCR and Western blotting to confirmed higher level of TSPO expression RPE/choroid when
316 compared to the retina (Fig. 8C-E). During retinal development, Wang et al detected highest TSPO
317 mRNA level in postnatal 0 (P0) retina, then significantly lower but steadily increased in postnatal age
318 (P0-P28), TSPO protein was also steadily increased in postnatal age (P0-P28) (25). However, another
319 group found TSPO mRNA was at highest level in P3 retina then continuously decreased to low levels
320 in adult (P60) retinas (44). We found that TSPO expression was markedly decreased in aged mouse
321 retina and RPE/choroid (Fig. 9A-C, Supplementary Material, Fig. S6B). Aged mouse RPE cells had
322 lower level of cholesterol efflux and higher level of total cholesterol (Fig. 9D, E), which may be in
323 part due to decreased TSPO, which appears to regulate cholesterol efflux in the RPE cells (Fig.2 and
324 Supplementary Material, Fig. S4).

325 Prevention of AMD progression is a priority in the long-term care of patients with early stage
326 disease. In pursuit of this objective several strategies are currently being investigated including high-
327 dose lipid lowering therapy (47) and laser-based interventions (48). Targeting the cholesterol efflux
328 pathway in order to ameliorate and/or reverse subretinal accumulation of lipid with associated RPE
329 dysfunction warrants further investigation. The availability of an approved TPSO ligand therapeutic
330 paves the way for translation to clinical trial. If safety and efficacy are demonstrated this novel
331 approach would usefully impact a key pathway likely to be involved in the complex process of
332 progression from early to late stage AMD. How modification of the TPSO pathway using a

333 biochemical approach or AAV-gene therapeutic might supplant or supplement other tools in reducing
334 the burden of AMD-related visual loss requires further study. Further we plan to investigate the role
335 of this pathway in other conditions which show sub-retinal deposits resembling AMD for example
336 late-onset retinal degeneration (49) and Sorsby fundus dystrophy (50).

337

338 **Materials and methods**

339 **Reagents**

340 Cell culture medium, trypsin, and penicillin/streptomycin were purchased from Lonza, UK.
341 Lipofectamine 2000 Transfection reagent, T-PER Tissue Protein Extraction, CellTracker™ Orange
342 CMTMR Dye, and Amplex® Red Cholesterol Assay were from Thermo Fisher Scientific, UK. ApoE,
343 ApoA-I, HDL and LDL were purchased from the Athens Research (USA). LDL, Oxidized LDL
344 (oxLDL) and fluorescence-labelled oxidized LDL (Dil-acLDL) were purchased from Alfa Aesar, UK.
345 Recombinant human TNF α , IL-1 β and human TNF- α and IL-1 β ELISA Development Kit were from
346 Peprotech, UK. Radiochemicals ([³H]cholesterol and [¹⁴C]acetic acid) and Scintillant were provided
347 by the ICN Biologicals. G418, TLC plate, phospholipids Assay, dispase II protease, Tri Reagent, and
348 tetrazolium salt were purchased from Sigma–Aldrich. Cas9 vector and gRNA vector were obtained
349 from Addgene, USA. Antibodies, TSPO (ab109497), CYP27A1 (Ab64889), LXR α (ab176323),
350 ABCA1 (ab7360), ABCG1 (ab52617), Alexa fluo 594 conjugated secondary antibody, and GAPDH
351 antibody were from Abcam. CYP46A1 and LDLR antibodies were from Novus Biologicals, UK.
352 Donkey anti mouse and donkey anti rabbit secondary antibodies were from Santa Cruz, UK. Mito
353 View™ Green was from Biotium, UK.

354 **Cell culture**

355 The human retinal pigment epithelium cell line (ARPE-19, ATCC® CRL-2302™) were maintained in
356 DMEM/F-12 medium supplemented with 10% (v/v) fetal bovine serum (FBS),
357 penicillin/streptomycin (50 μ g/ml and 50 IU/ml respectively) and 0.26% Sodium bicarbonate. For
358 experiments, cells were grown on to 48, 24, 12 and 6-well plates at density of 1×10^5 , 2×10^5 , 4×10^5
359 and 8×10^5 cells per well respectively.

360 **Cells viability**

361 The ARPE-19 cells (1×10^5 cells/well) were cultured in 48-well plates. The cells were treated with
362 different TSPO ligands (FGIN-1-27, XBD173, Etifoxine) in serum free media and incubated for 24
363 hours. Then the cells were washed with PBS and treated with serum-free medium containing 0.4
364 mg/mL MTT[3-(4, 5-dimethylthiazol-2-yl)-2,5-diphenyltetrazolium bromide]. During this period of
365 treatment, mitochondrial cytosolic dehydrogenases of living cells reduced the yellow tetrazolium salt
366 (MTT) to a purple formazan dye suitable for spectrophotometric detection. After 2 hours the MTT
367 solution was aspirated and dimethylsulfoxide (0.2 mL/well) was added to dissolve the formazan. The
368 plate was shaken for 10 minutes and then was read on a micro plate reader (EPOCH) at 575nm for
369 densities. The absorbance was normalised to untreated cells representing 100% cell viability.

370 **Measurement of [³H]cholesterol efflux**

371 Efflux of [³H]cholesterol to apoAI, apoE, HDL and human serum (HS) in RPE cells was determined
372 following previous description (8). Briefly, cells were seeded on 12 well plates and labelled with
373 [³H]cholesterol for 24 hours with 2% BSA in serum free culture media. Efflux was initiated by the
374 addition of serum-free DMEM/F12 containing human apoAI (10 µg/ml), apoE (10 µg/ml), HDL (20
375 µg/ml) or human serum (1%, v/v) and in the presence or absence TSPO ligands, and cultured for 24
376 hours. Cholesterol efflux was then calculated as an expression of percentage of cholesterol efflux to
377 each of the acceptors as follows: % efflux = (disintegrations per minute (DPM) media/DPM Media +
378 DPM Cells) × 100.

379 **Lipid analysis**

380 Incorporation of [¹⁴C]acetic acid (1 µCi/ml) into fatty acid, phospholipid, cholesterol, cholesteryl
381 ester and triacylglycerol pools was measured after incubation in the presence or absence of TSPO
382 ligands for 24 hours, as previously described (9,10). Cellular lipids were extracted using hexane:
383 isopropanol (3:2, v/v), dried under nitrogen gas and resuspended in isopropanol, before separation by
384 thin-layer chromatography (TLC) using mobile phase-I buffer (chloroform, methanol and water,
385 60:30:5, v/v/v) and mobile phase-II buffer (hexane, diethyl ether and acetic acid, 80:20:1.5, v/v/v).
386 Lipids were identified by co-migration with authentic standards and incorporation of radiolabel
387 assessed by scintillation counting. Mass of total cellular cholesterol and phospholipids in ARPE-19
388 cells was measured using an Amplex® Red Cholesterol Assay Kit (Thermo Fisher scientific)

389 according to the manufacturer's guidance. Total cholesterol mass of mouse RPE/choroid was
390 measured similarly.

391 **Measurement of reactive oxygen species (ROS)**

392 Wildtype and *TSPO*^{-/-} ARPE-19 cells were incubated with OxLDL (200µg/ml) for 4 h or 24 hours. To
393 detect intracellular ROS, cells were incubated for 30 minutes with the fluorescence dye carboxy-2',7'-
394 dichloro-dihydro- fluorescein diacetate (DCFHDA, Sigma, UK). The fluorescence signals were
395 measured at 485 nm (excitation) and 520 nm (emission) using FluoStar Optima MBG-Labtech
396 microplate reader. The ROS level was represented as fluorescence of treated cells) / fluorescence of
397 untreated cells.

398 **Enzyme-linked immunosorbent assay (ELISA)**

399 The cells were treated with oxLDL (200µg/ml) for 4 or 24hours. The levels of IL-1β and TNF-α in
400 culture medium were quantified by ELISA with human TNF-α and IL-1β kits (Peprotech, UK)
401 following the manufacturer's protocols.

402 **Uptake of oxidized LDL by RPE cells**

403 Fluorescence-labelled DiI-oxidized LDL (DiI-OxLDL) was purchased from Alfa Aesar, UK. ARPE-
404 19 cells were seeded in 6-well plates and treated with DiI-OxLDL (20µg/ml) for 4 or 24 hours. The
405 treated cells were washed five times with PBS and fixed with 4% PFA for 10 min at room
406 temperature then mounted with Vectashield medium with DAPI (Vector Lab Ltd. Peterborough, UK).
407 The intracellular fluorescence-labelled DiI-OxLDL was visualized by LSM 510 Zeiss confocal
408 microscope (Zeiss) and quantified using Image J.

409 **Flow cytometry**

410 The ARPE-19 cells were treated with DiI-labeled oxidized LDL (20µg/ml) for 4 hours and 24hrs.
411 Then the cells were washed 3 times with PBS and twice with PBS containing BSA (2 mg/ml). The
412 cells were collected by detachment in trypsin, resuspended with complete medium and centrifuged at
413 1000 rpm for 5 minutes and washed two times with PBS. The cells were analysed by flow cytometry
414 (10,000 events; Excitation, 514 nm; Emission; 550 nm) using a FACSCalibur BD Immunocytometry
415 Systems. The data were analyzed by FlowJo software (Treestar Inc).

416 **Knockout of *TSPO* in ARPE-19 cells**

417 The clustered regularly interspaced short palindromic repeats (CRISPR) system was employed to
418 knockout the *TSPO* gene from ARPE-19 cells. The CRISPR primers were designed using
419 <https://benchling.com> website to targeting exon 2 of *TSPO* gene (Accession: NC_018933). The
420 CRISPR Oligos were extended using Phusion DNA polymerase (New England Biolab, UK) and ligated
421 into linearized gRNA vector (Addgene 41824) using Gibson assembly to generate a CRISPR *TSPO*-
422 gRNA construct, which was confirmed by sequencing. The CRISPR *TSPO*-gRNA construct and Cas9
423 plasmid (Addgene 41815) were transfected into ARPE-19 cells. *TSPO* knockout colonies were
424 verified by Western blotting, Sanger sequencing and immunocytochemistry.

425 **Isolation of primary retinal pigment epithelium (RPE) cells from mouse eyes**

426 Eyes from 3-month and 20-month old mice were washed three times in PBS then washed twice in
427 DMEM F-12 medium. The eyes were transferred into HBSS solution and a circular incision was made
428 around the ora serrata of each eye. The lens and retina were removed, the RPE/choroid/sclera was
429 incubated with 2% dispase solution (w/v) in complete medium for 45 minutes at 37°C with 5 % CO₂.
430 The RPE/choroid/sclera was washed with PBS twice then incubated with trypsin-EDTA at 37°C for
431 15-20 minutes. After incubation the RPE/choroid/sclera was vigorously shaken to detach the RPE
432 cells. The detached RPE cells were cultured in DMEM F-12 medium until they reached confluent.

433 **Quantitative real-time polymerase chain reaction (qRT-PCR)**

434 Total RNA was extracted from ARPE-19 cells, mouse RPE/choroid, or mouse retinas using Tri
435 Reagent (Sigma, UK) according to the manufacturer's guidance. The cDNA was synthesised by using
436 High Capacity cDNA Reverse Transcription Kit with RNAase inhibitor (Applied Biosystems, UK).
437 The quantification of gene expression was performed by a qRT-PCR assay using a Platinum Syber
438 Green QAPCR Super Mix-UDG w/ROX kit (Invitrogen, UK) with primers for targeted genes.

439 **Immunocytochemistry and Immunohistology**

440 Wildtype and *TSPO*-deleted ARPE-19 cells were incubated with mitochondrial dye, MitoView Green
441 (100nM, Biotium, USA) in culture medium for 30 minutes at 37°C. After multiple washes with PBS,
442 the cells were fixed with 4% paraformaldehyde and blocked with 2% sheep serum with 2% BSA in
443 PBS then stained with a primary rabbit monoclonal *TSPO* antibody (Abcam ab109497, 1:200
444 dilution) which recognizes human *TSPO* C-terminal, and with secondary Alexa Fluor 594 secondary

445 antibody. In addition, mouse (three-month old) eyes were fixed with 4% paraformaldehyde in PBS
446 and cryoprotected in Cryomatrix medium (VWR, UK). The eyes were sectioned and mounted on
447 superfrost slides. The sections were blocked with 2% BSA in PBS and incubated with primary and
448 secondary antibodies. Images were captured using a LSM 510 confocal microscope (Zeiss).

449 **Western blotting**

450 Cell lysates were prepared in Radio-Immuno Precipitation Assay (RIPA) cell lysis buffer containing
451 25mM Tris-HCl pH8, 150mM Sodium Chloride, 1% (w/v) sodium deoxycholate, 1% (v/v)
452 nonylphenoxypolyethoxylethanol (NP-40), and 0.1% (w/v) sodium dodecyl sulphate supplemented
453 with Complete™ protease inhibitors (Roche). Mouse retina and RPE/choroid tissues were lysed using
454 T-PER™ tissue protein extraction reagent (Thermo Fisher Scientific, UK). Proteins were separated by
455 SDS-PAGE and transferred to nitrocellulose membranes. Target proteins were detected by incubation
456 with primary (1:2000 for TSPO and GAPDH; 1:200 for ABCA1, 1:1000 for ABCG1, CYP27A1 and
457 CYP46A1) and secondary (1:10000 dilution) antibodies. The intensity of specific bands was
458 quantified using Li-cor Odyssey FC and Image Studio software.

459 **Statistical Analysis**

460 Data was analysed by statistical significance using analysis of variance (ANOVA) and a t-test,
461 followed by appropriate post hoc tests (Bonferroni). As indicated, all data are presented as mean±SD
462 and collected from three independent experiments. Statistical analysis was performed using Prism
463 software (version 6.0 from GraphPad Software Inc., San Diego, CA, USA); *p<0.05, **p<0.01 and
464 ***p<0.001, ****p<0.0001.

465

466 **Acknowledgement**

467 We would like to thank the Rosetrees Trust, the Glasgow Children's Hospital Charity, the Fight for
468 Sight, and the Visual Research Trust for supporting this work.

469 Conflict of Interest statement. None declared.

470 **References**

- 471 1. Friedman, D.S., O'Colmain, B.J., Muñoz, B., Tomany, S.C., McCarty, C., de Jong, P.T., Nemesure,
472 B., Mitchell, P., Kempen, J., Eye Diseases Prevalence Research Group. (2004) Prevalence of age-
473 related macular degeneration in the United States. *Arch. Ophthalmol.*, **122**, 564–572.
- 474 2. Abdelsalam, A., Del Priore, L. and Zarbin, M.A. (1999) Drusen in age-related macular
475 degeneration: pathogenesis, natural course, and laser photocoagulation-induced regression.
476 *Surv. Ophthalmol.*, **44**, 1–29.
- 477 3. Guymer, R., Luthert, P. and Bird, A. (1999) Changes in Bruch's membrane and related structures
478 with age. *Prog. Retin. Eye Res.*, **18**, 59–90.
- 479 4. Curcio, C.A., Presley, J.B., Malek, G., Medeiros, N.E., Avery, D.V., Kruth, H.S. (2005) Esterified
480 and unesterified cholesterol in drusen and basal deposits of eyes with age-related maculopathy. *Exp.*
481 *Eye Res.*, **81**, 731-741.
- 482 5. Neale, B.M., Fagerness, J., Reynolds, R., Sobrin, L., Parker, M., Raychaudhuri, S., Tan, P.L., Oh,
483 E.C., Merriam, J.E., Souied, E. *et al.* (2010) Genome-wide association study of advanced age-related
484 macular degeneration identifies a role of the hepatic lipase gene (LIPC). *Proc. Natl. Acad. Sci. U.S.A.*,
485 **107**, 7395-7400.
- 486 6. Chen W, Stambolian D, Edwards AO, Branham KE, Othman M, Jakobsdottir J, Tosakulwong
487 N, Pericak-Vance MA, Campochiaro PA, Klein ML. *et al.* (2010) Genetic variants near TIMP3 and
488 high-density lipoprotein-associated loci influence susceptibility to age-related macular degeneration.
489 *Proc. Natl. Acad. Sci. U.S.A.*, **107**, 7401-7406.
- 490 7. Ikonen, E. (2006) Mechanisms for cellular cholesterol transport: defects and human disease.
491 *Physiol. Rev.*, 2006, 86, 1237-1261;
- 492 8. Taylor, J.M., Allen, A.M. and Graham, A. (2014) Targeting mitochondrial 18 kDa translocator
493 protein (TSPO) regulates macrophage cholesterol efflux and lipid phenotype. *Clin. Sci. (Lond.)*, **127**,
494 603-613.
- 495 9. Papadopoulos, V., Aghazadeh, Y., Fan, J., Campioli, E., Zirkin, B., Midzak, A. (2015) Translocator
496 protein-mediated pharmacology of cholesterol transport and steroidogenesis. *Mol. Cell Endocrinol.*,
497 **408**, 90-98.

498 10. Fan, J., Campioli, E., Midzak, A., Culty, M., Papadopoulos, V. (2015) Conditional steroidogenic
499 cell-targeted deletion of TSPO unveils a crucial role in viability and hormone-dependent steroid
500 formation. *Proc. Natl. Acad. Sci. U.S.A.*, **112**, 7261-7266

501 11. Morohaku, K., Pelton, S.H., Daugherty, D.J., Butler, W.R., Deng, W., Selvaraj, V. (2014)
502 Translocator protein/peripheral benzodiazepine receptor is not required for steroid hormone
503 biosynthesis. *Endocrinology*, **155**, 89-97.

504 12. Tu, L.N., Morohaku, K., Manna, P.R., Pelton, S.H., Butler, W.R., Stocco, D.M., Selvaraj, V.
505 (2014) Peripheral benzodiazepine receptor/translocator protein global knock-out mice are viable with
506 no effects on steroid hormone biosynthesis. *J. Biol. Chem.*, **289**, 27444-22454.

507 13. Ishida, B.Y., Duncan, K.G., Bailey, K.R., Kane, J.P., Schwartz, D.M. (2006) High density
508 lipoprotein-mediated lipid efflux from retinal pigmented epithelial cells in culture. *Br. J.*
509 *Ophthalmol.*, **90**, 616–620.

510 14. Lakkaraju, A., Finnemann, S.C. and Rodriguez-Boulan, E. (2007) The lipofuscin fluorophore A2E
511 perturbs cholesterol metabolism in retinal pigment epithelial cells. *Proc. Natl. Acad. Sci. U.S.A.*, **104**,
512 11026-11031.

513 15. Feeney-Burns, L., Hilderbrand, E.S., Eldridge, S. (1984) Aging human RPE: morphometric
514 analysis of macular, equatorial, and peripheral cells. *Invest. Ophthalmol. Vis. Sci.* **25**, 95-200.

515 16. Tserentsoodol, N., Gordiyenko, N.V., Pascual, I., Lee, J.W., Fliesler, S.J., Rodriguez, I.R. (2006)
516 Intraretinal lipid transport is dependent on high density lipoprotein-like particles and class B
517 scavenger receptors. *Mol. Vis.*, **12**, 1319-1333.

518 17. Zareparsari, S., Buraczynska, M., Branham, K.E., Shah, S., Eng, D., Li, M., Pawar, H., Yashar,
519 B.M., Moroi, S.E., Lichter, P.R. et al. (2005) Toll-like receptor 4 variant D299G is associated with
520 susceptibility to age-related macular degeneration. *Hum. Mole. Genet.*, **14**, 1449-1455.

521 18. Ishida, B.Y., Bailey, K.R., Duncan, K.G., Chalkley, R.J., Burlingame, A.L., Kane, J.P., Schwartz,
522 D.M. (2004) Regulated expression of apolipoprotein E by human retinal pigment epithelial cells. *J.*
523 *Lipid Res.*, **45**, 263–271.

- 524 19. Li, C.M., Chung, B.H., Presley, J.B., Malek, G., Zhang, X., Dashti, N., Li, L., Chen, J., Bradley,
525 K., Kruth, H.S. *et al.* (2005) Lipoprotein-like particles and cholesteryl esters in human Bruch's
526 membrane: initial characterization. *Invest. Ophthalmol. Vis. Sci.*, **46**, 2576-2586.
- 527 20. Cosenza-Nashat, M., Zhao, M.L., Suh, H.S., Morgan, J., Natividad, R., Morgello, S., Lee, S.C.
528 (2009) Expression of the translocator protein of 18 kDa by microglia, macrophages and astrocytes
529 based on immunohistochemical localization in abnormal human brain. *Neuropathol. Appl.*
530 *Neurobiol.*, **35**, 306–328.
- 531 21. Falchi, A.M., Battetta, B., Sanna, F., Piludu, M., Sogos, V., Serra, M., Melis, M., Putzolu, M.,
532 Diaz, G. (2007) Intracellular cholesterol changes induced by translocator protein (18 kDa) TSPO/PBR
533 ligands. *Neuropharmacology*, **53**, 318-329.
- 534 22. Ji, B., Maeda, J., Sawada, M., Ono, M., Okauchi, T., Inaji, M., Zhang, M.R., Suzuki, K.,
535 Ando, K., Staufenbiel, M. *et al.* (2008) Imaging of peripheral benzodiazepine receptor expression as
536 biomarkers of detrimental versus beneficial glial responses in mouse models of Alzheimer's and other
537 CNS pathologies. *J. Neurosci.*, **28**, 12255–12267.
- 538 23. Karlstetter, M., Nothdurfter, C., Aslanidis, A., Moeller, K., Horn, F., Scholz, R., Neumann, H.,
539 Weber, B.H., Rupprecht, R., Langmann, T. (2014) Translocator protein (18 kDa) (TSPO) is expressed
540 in reactive retinal microglia and modulates microglial inflammation and phagocytosis. *J.*
541 *Neuroinflammation*, **11**, 3.
- 542 24. Stephenson, D.T., Schober, D.A., Smalstig, E.B., Mincy, R.E., Gehlert, D.R., Clemens, J.A.
543 (1995) Peripheral benzodiazepine receptors are colocalized with activated microglia following
544 transient global forebrain ischemia in the rat. *J. Neurosci.*, **15**, 5263–5274.
- 545 25. Wang, M., Wang, X., Zhao, L., Ma, W., Rodriguez, I.R., Fariss, R.N., Wong, W.T. (2014)
546 Macrogliia-microglia interactions via TSPO signaling regulates microglial activation in the
547 mouse retina. *J. Neurosci.*, **34**, 3793-3806.
- 548 26. Tserentsoodol, N., Szein, J., Campos, M., Gordiyenko, N.V., Fariss, R.N., Lee, J.W., Fliesler,
549 S.J., Rodriguez, I.R. (2006) Uptake of cholesterol by the retina occurs primarily via a low density
550 lipoprotein receptor-mediated process. *Mol. Vis.*, **12**, 1306-1318.

551 27. Zheng, W., Reem, R.E., Omarova, S., Huang, S., DiPatre, P.L., Charvet, C.D., Curcio,
552 C.A., Pikuleva, I.A. (2012) Spatial distribution of the pathways of cholesterol homeostasis in human
553 retina. *PLoS. One*, **7**, e37926.

554 28. Maiolino, G., Rossitto, G., Caielli, P., Bisogni, V., Rossi, G.P., Calò, L.A. (2013) The role of
555 oxidized low-density lipoproteins in atherosclerosis: the myths and the facts. *Mediators Inflamm.*,
556 **2013**, 714653.

557 29. Ma, K.L., Ruan, X.Z., Powis, S.H., Chen, Y., Moorhead, J.F., Varghese, Z. (2008) Inflammatory
558 stress exacerbates lipid accumulation in hepatic cells and fatty livers of apolipoprotein E knockout
559 mice. *Hepatology*, **48**, 770-781.

560 30. Ruan, X.Z., Moorhead, J.F., Tao, J.L., Ma, K.L., Wheeler, D.C., Powis, S.H., Varghese, Z. (2006)
561 Mechanisms of dysregulation of low-density lipoprotein receptor expression in vascular smooth
562 muscle cells by inflammatory cytokines. *Arterioscler. Thromb. Vasc. Biol.*, **26**, 1150-1155.

563 31. Tu, L.N., Zhao, A.H., Hussein, M., Stocco, D.M., Selvaraj, V. (2016) Translocator protein
564 (TSPO) affects mitochondrial fatty acid oxidation in steroidogenic cells. *Endocrinology*, **157**, 1110-
565 1121.

566 32. Pikuleva, I.A. and Curcio, C.A. (2014) Cholesterol in the retina: the best is yet to come. *Prog.*
567 *Retin. Eye Res.*, **41**, 64-89.

568 33. Sene, A., Khan, A.A., Cox, D., Nakamura, R.E., Santeford, A., Kim, B.M., Sidhu, R., Onken,
569 M.D., Harbour, J.W., Hagbi-Levi, S. *et al* (2013) Impaired cholesterol efflux in senescent
570 macrophages promotes age-related macular degeneration. *Cell Metabolism*, **17**, 549-561.

571 34. Graham, A. (2015) Mitochondrial regulation of macrophage cholesterol homeostasis. *Free Radic.*
572 *Biol. Med.*, **89**, 982-992.

573 35. Li, F., Liu, J., Liu, N., Kuhn, L.A., Garavito, R.M., Ferguson-Miller, S. (2016) Translocator
574 protein 18 kDa (TSPO): an old protein with new functions? *Biochemistry*, **55**, 2821-2831.

575 36. Curcio, C.A., Johnson, M., Huang, J.D., Rudolf, M. (2009) Aging, age-related macular
576 degeneration, and the response-to-retention of apolipoprotein B-containing lipoproteins. *Prog. Retin.*
577 *Eye Res.*, **28**, 393-422.

578 37. Yamada, Y., Tian, J., Yang, Y., Cutler, R.G., Wu, T., Telljohann, R.S., Mattson, M.P., Handa, J.T.
579 (2008) Oxidized low density lipoproteins induce a pathologic response by retinal pigmented epithelial
580 cells. *J Neurochem.*, **105**, 1187-1197.

581 38. Gordiyenko, N., Campos, M., Lee, J.W., Fariss, R.N., Sztejn, J., Rodriguez, I.R. (2004) RPE cells
582 internalize low-density lipoprotein (LDL) and oxidized LDL (oxLDL) in large quantities in vitro and
583 in vivo. *Invest. Ophthalmol. Vis. Sci.*, **45**, 2822-2829.

584 39. Hoppe, G., Marmorstein, A.D., Pennock, E.A., Hoff, H.F. (2001) Oxidized low density
585 lipoprotein-induced inhibition of processing of photoreceptor outer segments by RPE. *Invest.*
586 *Ophthalmol. Vis. Sci.*, **42**, 2714-2720.

587 40. Hoppe, G., O'Neil, J., Hoff, H.F., Sears, J. (2004) Accumulation of oxidized lipid-protein
588 complexes alters phagosome maturation in retinal pigment epithelium. *Cell Mol. Life Sci.*, **61**, 1664-
589 1674.

590 41. Ebrahimi, K.B., Fijalkowski, N., Cano, M., Handa, J.T. (2013) Decreased membrane complement
591 regulators in the retinal pigmented epithelium contributes to age-related macular degeneration. *J.*
592 *Pathol.*, **229**, 729-742.

593 42. Tan, L.X., Toops, K.A., Lakkaraju, A. (2016) Protective responses to sublytic complement in the
594 retinal pigment epithelium. *Proc. Natl. Acad. Sci. U.S.A.*, **113**, 8789-8794.

595 43. Dupont, A.C., Largeau, B., Santiago Ribeiro, M.J., Guilloteau, D., Tronel, C., Arlicot, N. (2017)
596 Translocator Protein-18 kDa (TSPO) Positron Emission Tomography (PET) Imaging and Its Clinical
597 Impact in Neurodegenerative Diseases. *Int. J. Mol. Sci.*, **18**, pii: E785.

598 44. Karlstetter, M., Nothdurfter, C., Aslanidis, A., Moeller, K., Horn, F., Scholz, R., Neumann, H.,
599 Weber, B.H., Rupprecht, R., Langmann, T. (2014) Translocator protein (18 kDa) (TSPO) is expressed
600 in reactive retinal microglia and modulates microglial inflammation and phagocytosis. *J.*
601 *Neuroinflammation*, **11**, 3.

602 45. Scholz, R., Caramoy, A., Bhuckory, M.B., Rashid, K., Chen, M., Xu, H., Grimm, C., Langmann,
603 T. (2015) Targeting translocator protein (18 kDa) (TSPO) dampens pro-inflammatory microglia
604 reactivity in the retina and protects from degeneration. *J. Neuroinflammation*, **12**, 201.

605 46. Ishikawa, M., Yoshitomi, T., Covey, D.F., Zorumski, C.F., Izumi, Y. (2016) TSPO activation
606 modulates the effects of high pressure in a rat ex vivo glaucoma model. *Neuropharmacology*, **111**,
607 142-159.

608 47. Vavvas, D.G., Daniels, A.B., Kapsala, Z.G., Goldfarb, J.W., Ganotakis, E., Loewenstein, J.I.,
609 Young, L.H., Gragoudas, E.S., Elliott, D., Kim, I.K.. *et al.* (2016) Regression of some high-risk
610 features of age-related macular degeneration (AMD) in patients receiving intensive statin treatment.
611 *EBioMedicine*, **5**, 198-203.

612 48. Jobling, A.I., Guymer, R.H., Vessey, K.A., Greferath, U., Mills, S.A., Brassington, K.H., Luu,
613 C.D., Aung, K.Z., Trogrlic, L., Plunkett, M. *et al.* (2015) Nanosecond laser therapy reverses
614 pathologic and molecular changes in age-related macular degeneration without retinal damage.
615 *FASEB. J.*, **29**, 696-710.

616 49. Hayward, C., Shu, X., Cideciyan, A.V., Lennon, A., Barran, P., Zarepari, S., Sawyer, L., Hendry,
617 G., Dhillon, B., Milam, A.H. *et al.* Mutation in a short-chain collagen gene, CTRP5, results in
618 extracellular deposit formation in late-onset retinal degeneration: a genetic model for age-related
619 macular degeneration. *Hum. Mol. Genet.*, **12**, 2657-2667.

620 50. Gliem, M., Müller, P.L., Mangold, E., Holz, F.G., Bolz, H.J., Stöhr, H., Weber, B.H., Charbel
621 Issa, P. (2015) Sorsby Fundus Dystrophy: Novel Mutations, Novel Phenotypic Characteristics, and
622 Treatment Outcomes. *Invest. Ophthalmol. Vis. Sci.*, **56**, 2664-2676.

623
624
625
626
627
628
629
630
631
632

633 **Legends to Figures**

634 **Figure 1** TSPO localization in ARPE-19 cells. ARPE-19 cells were incubated with MitoView
635 (mitochondria marker) and fixed with cold methanol, then incubated with anti-TSPO antibody and
636 secondary antibody. TSPO was colocalized with MitoView in mitochondria.

637

638 **Figure 2** Cholesterol acceptor-mediated cholesterol efflux was measured from ARPE-19 cells. The
639 cells were treated with TSPO ligand, FGIN-1-27 (10 μ M), XBD137 (25 μ M) or Etifoxine (20 μ M) for
640 24 hours. The percentage of [3 H] cholesterol efflux was measured from the medium and the cellular
641 lipids. Data was presented as means \pm SD. Every experiment was performed in triplicate and three
642 independent experiments were carried out. NS: non-significant, * p <0.05, ** p <0.01, **** p <0.0001:

643

644 **Figure 3** TSPO ligand modulation of lipids phenotypes. A-C Impact of TSPO ligands (Fgin-1-27,
645 XBD173 and Etifoxine) on nmol incorporation per mg total protein of [14 C] acetate (1 μ Ci/ml) into
646 phospholipid, triacylglycerol, cholesteryl ester, free cholesterol and fatty acid pools compared with
647 the vehicle control. The incorporation of radiolabel was normalised to mg total cellular protein. The
648 effect of TSPO ligands on the ARPE-19 total cholesterol (D) and phospholipids mass (E) were
649 reduced significantly due to expose to TSPO ligands for 24 hours. Values of total cholesterol and
650 phospholipids from above experiments were normalised based on total cellular protein. Three
651 independent experiments were performed. ** p <0.01, *** p <0.001, **** p <0.0001.

652

653 **Figure 4** CRISPR/Cas9 system mediated knockout of *TSPO* from ARPE-19 cells. (A) Schematic
654 structure of *TSPO* gene, the targeting sequence and the protospacer adjacent motif (PAM) were
655 shown. (B) After transfection with TSPO-CRISPR/Cas9 construct, ARPE-19 colonies were screened
656 for TSPO protein expression using a monoclonal TSPO antibody. Two TSPO-deleted colonies (KO1
657 and KO2) were identified by Western blotting. (C) Immunocytochemistry also confirmed the
658 complete absence of TSPO from mitochondria (MitView Green) in knockout ARPE-19 cells.

659

660 **Figure 5** Significantly increased cholesterol accumulation and uptake in *TSPO*^{-/-} cells. The wildtype
661 and *TSPO*^{-/-} ARPE-19 cells were incubated with DiI-oxLDL_a (20μg/ml) for 4 hours or 24 hours. The
662 intracellular oxLDL was detected by confocal microscopy and also assessed by fluorescence-activated
663 cell sorting (FACS). (A) Confocal image showing more oxLDL accumulation in TSPO deleted RPE
664 cells. (B) Quantification of fluorescence signals by using Image J software showing significant
665 increase of oxLDL accumulation in *TSPO*^{-/-} cells when compared to wildtype cells. (C) FACS
666 showing significant increase of fluorescence intensity in *TSPO*^{-/-} RPE cells when compared to the
667 wildtype cells exposed to oxLDL for 24 hours (p<0.001). (D) Confocal image showing increased
668 uptake of oxLDL. (E) Quantification of the increase using Image J software confirming the increase
669 of uptake by 34% in TSPO knockout cells. (F) FACS showing marked increase of oxLDL uptake in
670 TSPO-deleted cells (p<0.001). **p<0.01, ***p<0.001.

671

672 **Figure 6** The expression of LDLR was quantified after exposure to oxLDL. (A) After 4 hours
673 incubated with oxLDL, mRNA level of *LDLR* was increased 2341 fold in *TSPO* knockout cells
674 compared to wild type cells as well as protein level also increased significantly (B). Similarly, after 24
675 hours incubation of oxLDL, *LDLR* mRNA (C) and protein (D) were significantly increased. Data
676 were presented as mean±SD. NS: no significance, *p<0.05, **p<0.01, ***p<0.001.

677

678 **Figure 7** Significantly increased reactive oxygen species (ROS) and inflammatory cytokines levels in
679 TSPO-deleted RPE cells. Wildtype (WT) and *TSPO* knockout (KO) ARPE-19 cells were exposed to
680 oxLDL (200μg/ml) or vehicle control for 4 or 24 hours. (A) Cellular ROS levels were increased
681 markedly after treated with oxLDL (4 hours), however in TSPO-deleted cells ROS were remarkably
682 higher than that of wildtype cells. Similarly, marked increase of ROS also occurred in *TSPO* knockout
683 cells after 24 hours exposure to oxLDL (B). The levels of the inflammatory cytokines (IL-1β and
684 TNFα) were significantly increased TSPO deleted cells after exposure to oxLDL for 4 or 24 hours (C,
685 D). NS: no significance, *p<0.05, **p<0.01, ***p<0.001, ****p<0.0001.

686

687 **Figure 8** TSPO protein in mouse retina and RPE/choroid. Three-month old mouse eye sections were
688 immunostained with an TSPO antibody for TSPO expression and DAPI for labelling nuclei. (A)
689 Immunolocalization of TSPO in choroid, retinal pigment epithelium (RPE), outer nuclear layer
690 (ONL), and inner nuclear layer (INL). Strong TSPO signals were presented in the RPE layer. (B)
691 TSPO signals detected in ganglial cells layer (GCL). Retina and RPE/choroid (RC) were lysed to
692 quantify TSPO expression at mRNA and protein levels. Both mRNA (C) and protein (D, E) of TSPO
693 were significantly higher in RPE/RC than that of the retina. Data were presented as mean±SD.
694 ***p<0.001.

695

696 **Figure 9** TSPO expression, total cholesterol and cholesterol efflux in aged mouse RPE. (A) mRNA of
697 *Tspo* expression was significantly decreased in 20-month old mouse RPE cells. (B, C) TSPO protein
698 in RPE cell derived from 20-month old mice was also significantly decreased. TSPO protein intensity
699 was normalized to GAPDH. (D) Total cholesterol contents of RPE cells derived from 3-month or 20-
700 month mice were measured and normalized to total protein contents. RPE cells from 20-month old
701 mice had marked higher level of total cholesterol when compared to RPE cells from 3-month old
702 mice. (E) RPE cell derived from 3 or 20 months old mice were labelled with 0.5µCi/mL [³H]
703 cholesterol for 24 hours followed by 24 hours incubation with or without Apo A-I (10µg/ml), HDL
704 (20µg/ml) and human serum (HS, 1% v/v). After incubation, the percentage of [³H]cholesterol efflux
705 was measured. RPE cells from aged (20-month old) had significant decrease in cholesterol efflux to
706 ApoAI, HDL and human serum.

707

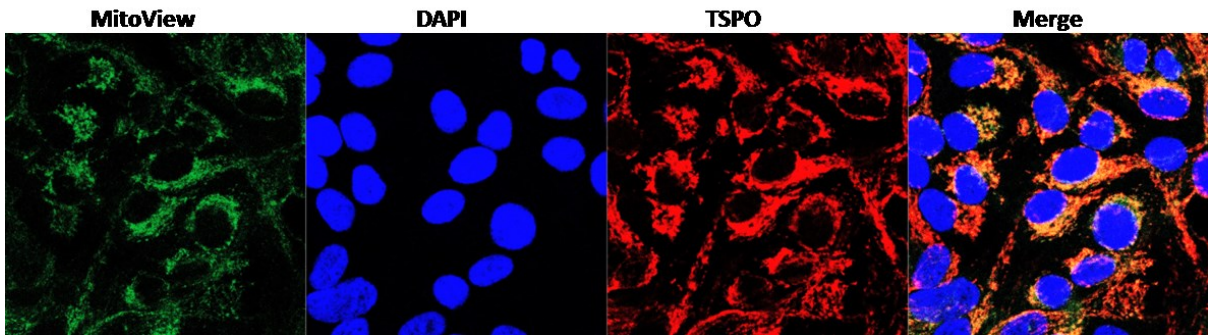
708 **Abbreviations**

709 ABCA1: ATP binding cassette subfamily A member 1; ABCG1: ATP binding cassette subfamily G
710 member 1; AMD: age related macular degeneration; CETP: cholesteryl ester transfer protein; HDL:
711 high-density lipoprotein; LDL, low-density lipoprotein; LIPC: hepatic lipase C; RPE retinal pigment
712 epithelium; TSPO translocator protein.

713

714 Figures

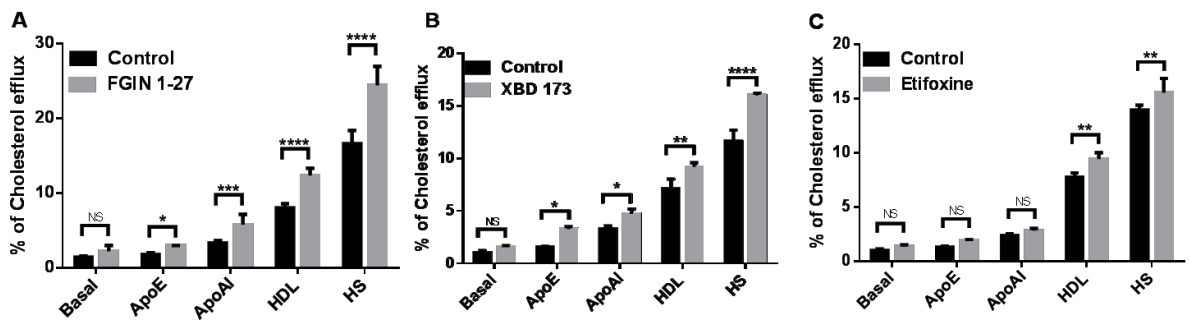
715 Figure 1



716

717

718 Figure 2



719

720

721

722

723

724

725

726

727

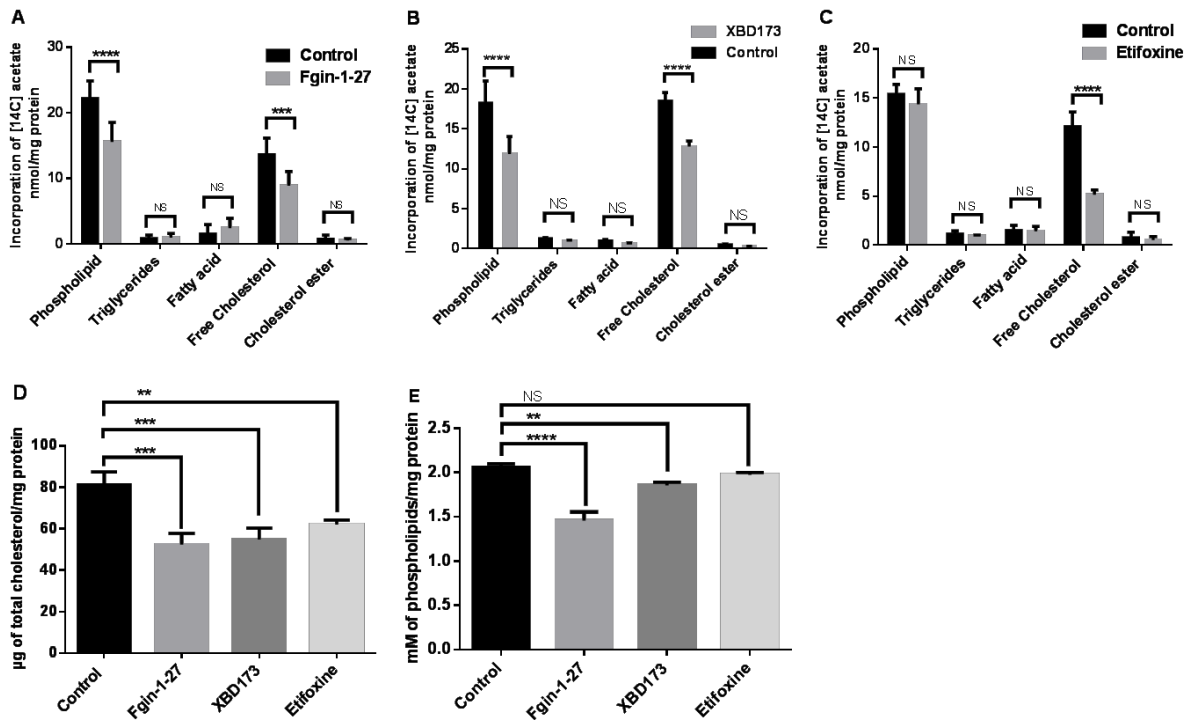
728

729

730

731

732 **Figure 3**



733

734

735

736

737

738

739

740

741

742

743

744

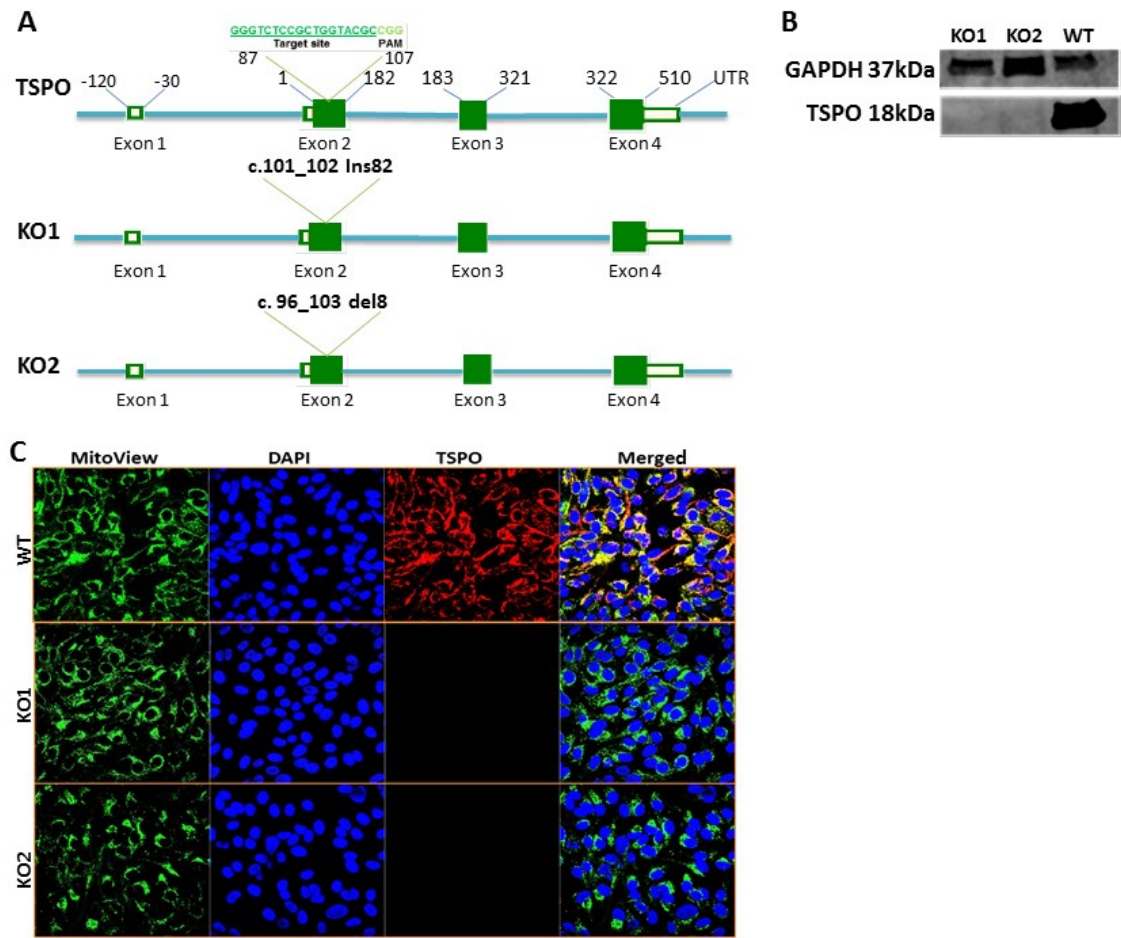
745

746

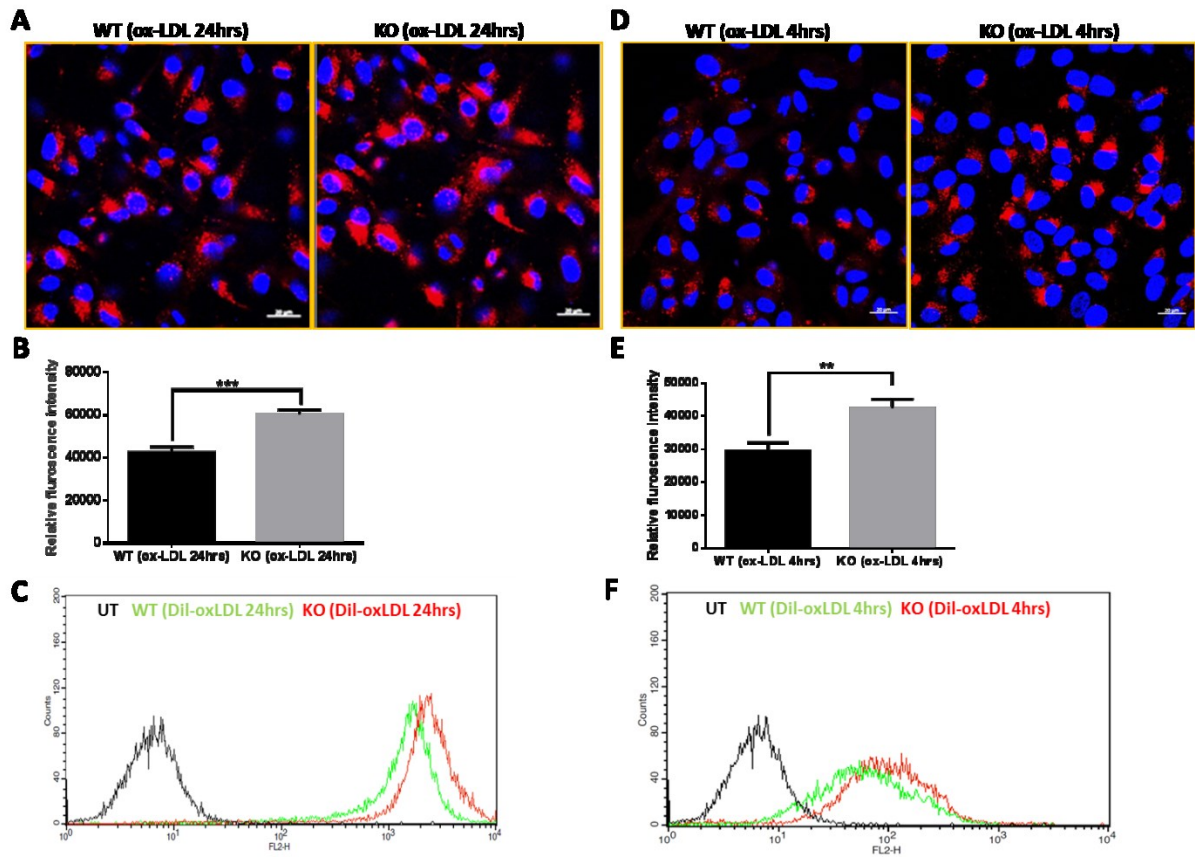
747

748

749 **Figure 4**



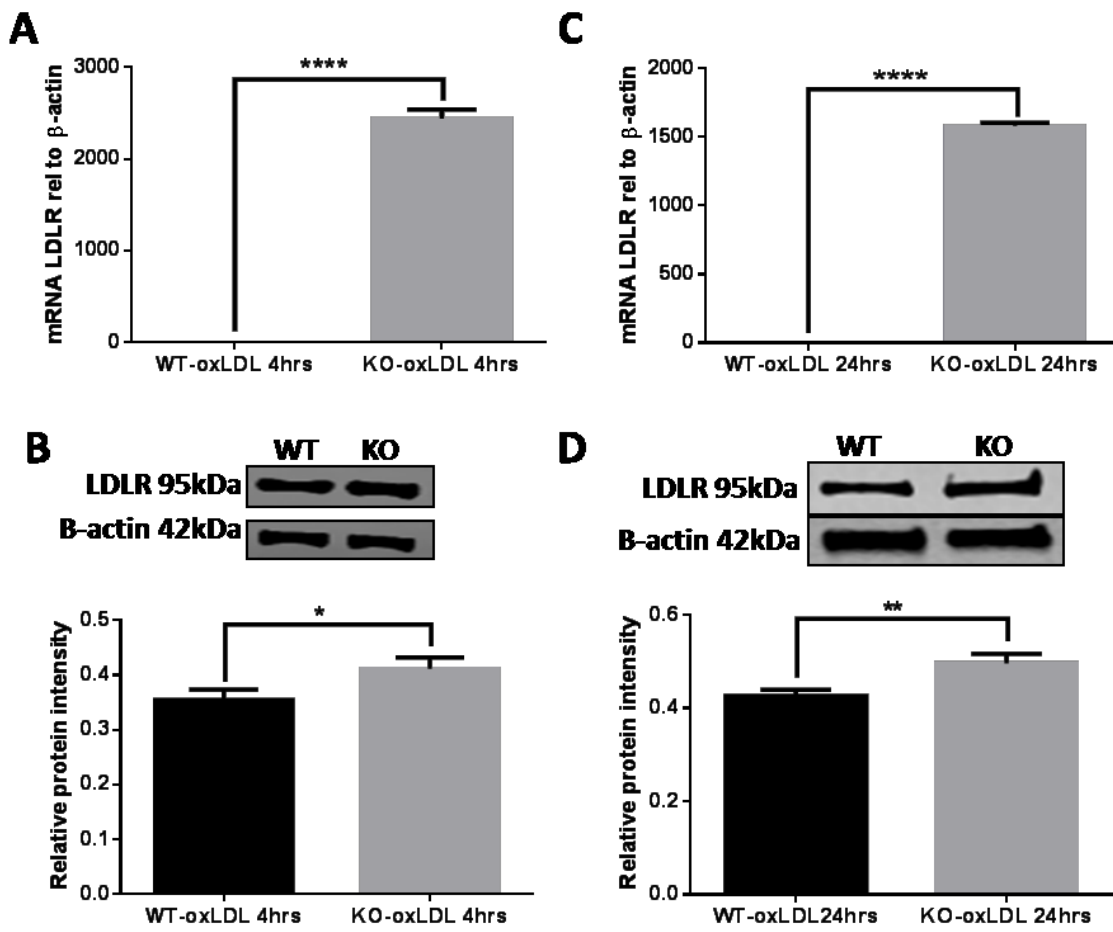
750
751
752
753
754
755
756
757
758
759
760
761
762



764
765
766
767
768
769
770
771
772
773
774
775
776
777

778

779 **Figure 6**



780

781

782

783

784

785

786

787

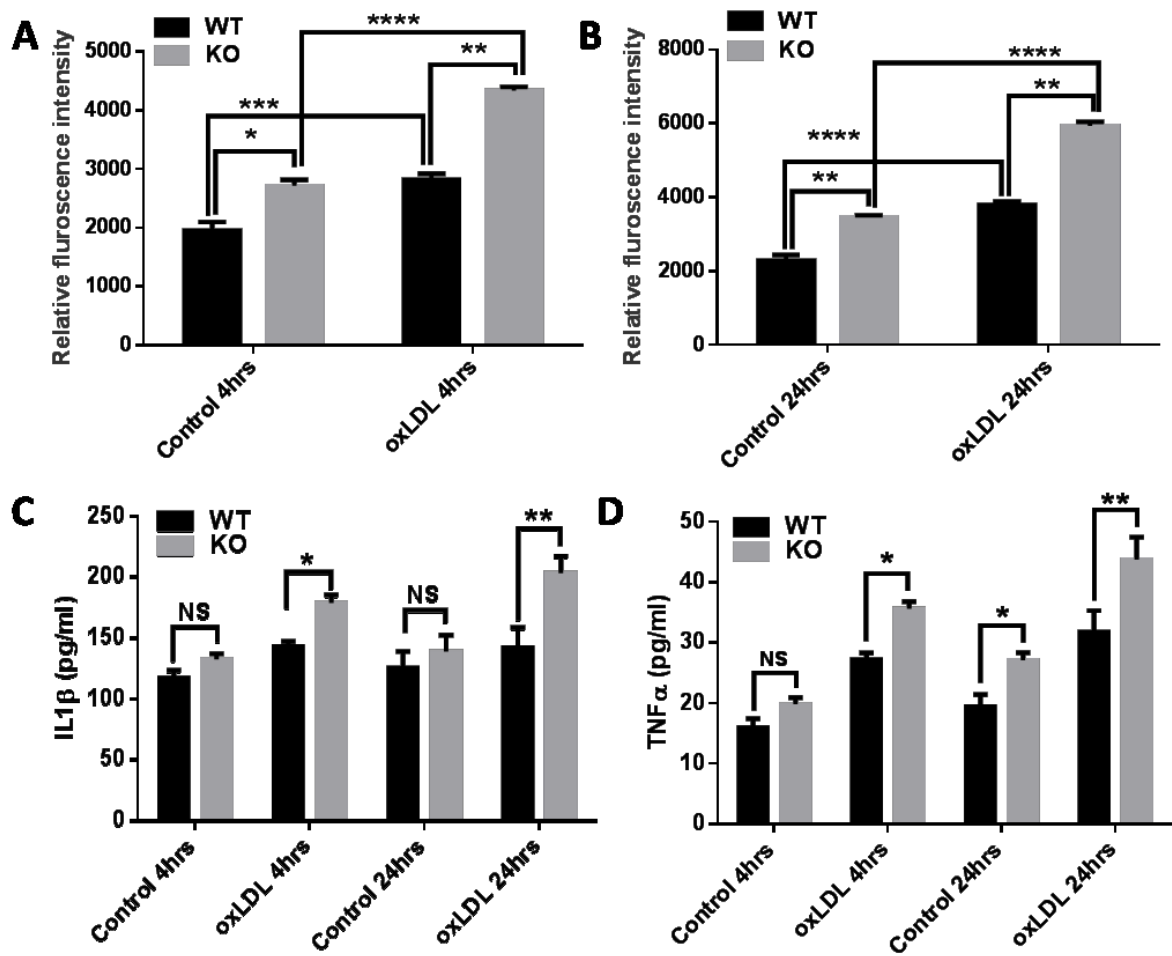
788

789

790

791

792 Figure 7



793

794

795

796

797

798

799

800

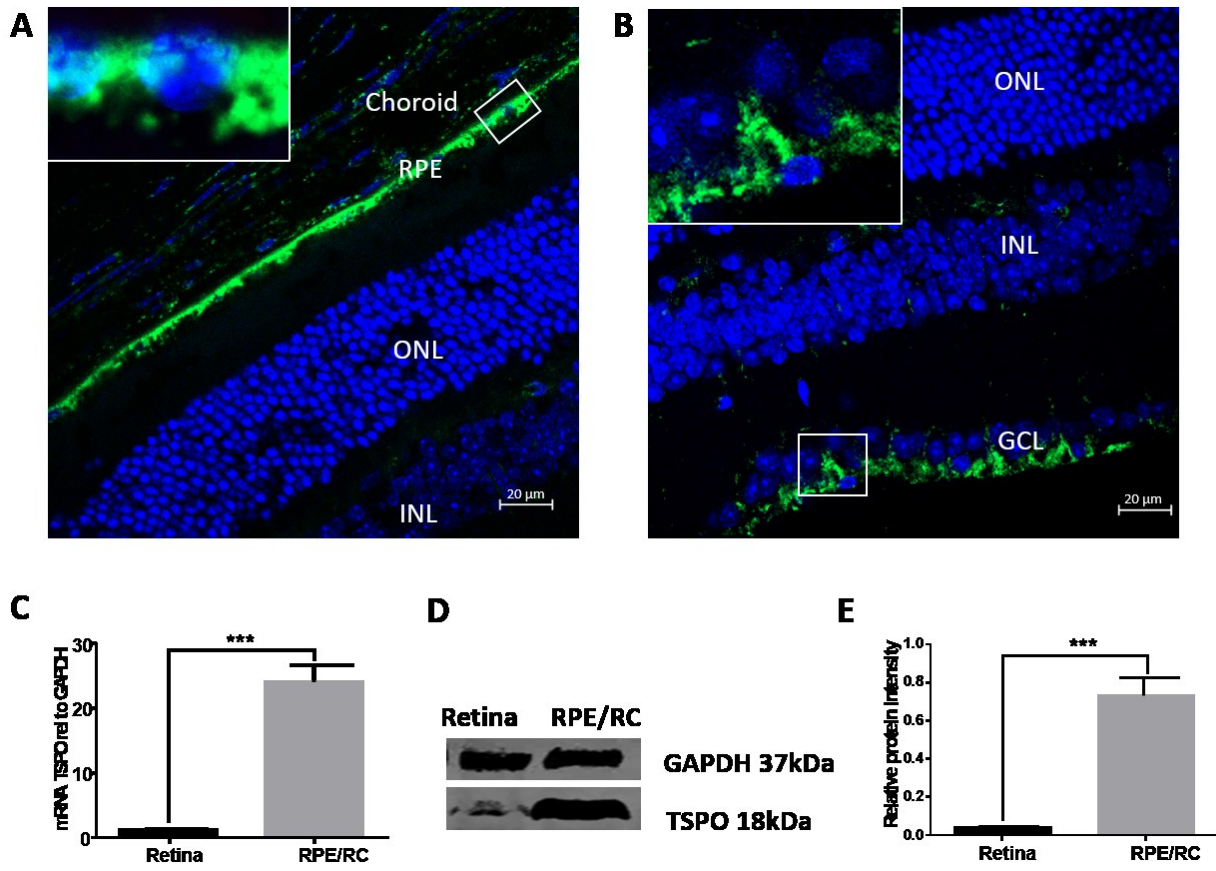
801

802

803

804

805 **Figure 8**



806

807

808

809

810

811

812

813

814

815

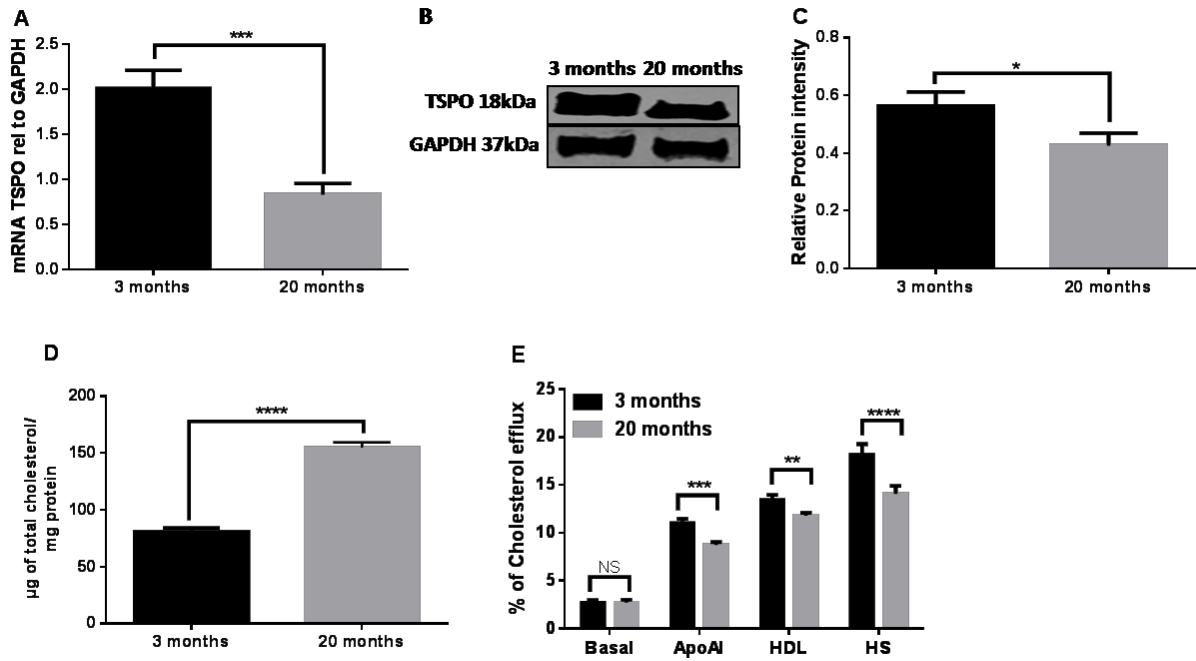
816

817

818

819

820 **Figure 9**



821

822

823

824